OpenAIR @RGU ROBERT GORDON UNIVERSITY ABERDEEN

This publication is made freely available under GREEN open access.

AUTHOR(S): XU, H., SONG, P., FERNANDEZ, C., WANG, J., SHIRAISHI, Y., WANG, C. and DU, Y.

TITLE: Surface plasmon enhance ethylene glycol electrooxidation based on hollow platinum-silver nanodendrites.

YEAR: 2018

Publisher citation: XU, H., SONG, P., FERNANDEZ, C., WANG, J., SHIRAISHI, Y., WANG, C. and DU, Y. 2018. Surface plasmon enhance ethylene glycol electrooxidation based on hollow platinum-silver nanodendrites. Journal of the Taiwan Institute of Chemical Engineers [online], 91, pages 316-322. Available from: https://doi.org/10.1016/j.jtice.2018.05.036

OpenAIR citation: XU, H., SONG, P., FERNANDEZ, C., WANG, J., SHIRAISHI, Y., WANG, C. and DU, Y. 2018. Surface plasmon enhance ethylene glycol electrooxidation based on hollow platinum-silver nanodendrites. Journal of the Taiwan Institute of Chemical Engineers, 91, pages 316-322. Held on OpenAIR [online]. Available from: https://openair.rgu.ac.uk

Publisher copyright statement:

This is the AUTHOR ACCEPTED version of an article originally published by ELSEVIER in Journal of the Taiwan Institute of Chemical Engineers (ISSN 1876-1070; eISSN _____).

OpenAIR takedown statement:

Section 6 of the "Repository policy for OpenAIR @ RGU" (available from http://www.rgu.ac.uk/staff-and-current-students/library/library-policies/repository-policies) provides guidance on the criteria under which RGU will consider withdrawing material from OpenAIR. If you believe that this item is subject to any of these criteria, or for any other reason should not be held on OpenAIR, then please contact openair-help@rgu.ac.uk with the details of the item and the nature of your complaint.

This publication is distributed under a CC BY-NC-ND 4.0 license.

https://creativecommons.org/licenses/by-nc-nd/4.0

OpenAIR at RGU Digitally signed by OpenAIR at RGU Date: 2018.10.11 15:48:30 +01'00'

*Highlight (for review)

Highlights

1. The dendritic Pt-Ag hollow nanocrystals have been successfully engineered.
2. Plasmonic nanostructures can serve as highly efficient photocatalysts.
3. Surface plasmon resonance enhance photoelectrocatalytic EGOR.
4. Facile design over the plasmonic metals endow them superior catalytic activity.

*Manuscript
Click here to view linked References

Surface plasmon enhanced ethylene glycol electrooxidation based on hollow platinum-silver nanodendrites structures

Hui Xu,[a] Pingping Song,[a] Carlos Fernandez,[b*] Jin Wang,[a] Yukihide Shiraishi,[c] Caiqin Wang [a, d*] and Yukou Du [a, c*]

[a]*College of Chemistry, Chemical Engineering and Materials Science, Soochow University, Suzhou 215123, PR China*

[b]*School of Pharmacy and Life Sciences Robert Gordon University U K*

[c]*Tokyo University of Science Yamaguchi, Sanyo-Onoda-shi, Yamaguchi 756-0884, Japan*

[d]*Chemistry Department, University of Toronto, Toronto M5S3H4, RP Canada*

** Corresponding author: Tel: 86-512-65880089, Fax: 86-512-65880089;*

E-mail: duyk@suda.edu.cn (Y. Du).

Abstract

The surface plasmon resonance (SPR) effect on noble metals to convert solar energy into chemical has attracted a lot of interest. However, the lack of highly efficient photocatalysts is still the forbidden obstacle as well as their large-scale development. Therefore, we focus on plasmon resonance enhanced electrocatalytic oxidation of liquid fuel employing photocatalysts to develop unique hollow platinum-silver (Pt-Ag) nanocrystals. The hollow Pt-Ag is formed of nanodendrites (Pt_1-Ag_1) which display a great enhancement in catalytic activity towards ethylene glycol oxidation with the mass and specific activity found to be: 7045.2 mA mg^{-1} and 14.1 mA cm^{-2}, respectively. This is due to: the SPR effect, efficient electronic distribution and synergistic properties, together with the unique hollow dendritic nanostructures. Impressively, the SPR effect also induces the optimum Pt-Ag nanocatalsyst under visible light irradiation conditions to display 1.7-fold enhancements in catalytic activity compared to that under dark conditions. In addition, 6.2 and 7.0-fold enhancements were obtained when the optimized Pt-Ag was employed as photoelectrocatalyst compared to the commercial Pt/C. Therefore, we present a unique catalyst which produces a high catalytic activity and long-term stability compared to those previously reported. More importantly, we also introduce a promising approach towards the designing of a plasmonic metal nanocatalyst with ideal nanostructures for liquid fuel oxidations.

Keywords: Plasmonic nanostructures; SPR effect; Hollow Pt-Ag dendrites; Ethylene glycol oxidation; Visible light

1. Introduction

The production and conversion of solar energy have received much attention in recent years [1]. The use of different photocatalysts to directly convert solar energy into chemical has attracted a great interest. Although most of the photocatalysts are semiconductors, it has also been well demonstrated that plasmonic nanostructures of noble metals such as gold and silver also serve as efficient photocatalysts [2, 3]. Plasmonic metallic nanostructures are featured with their strong interactions with resonant photons *via* exciting the SPR [4, 5]. In addition, the SPR can be characterized by the collective oscillation of valence electrons induced by resonance photons [6, 7]. Therefore, the investigation of SPR induced photoelectrocatalytic effect based on plasmonic metallic nanostructures is of vital significance for exploring highly efficient photoelectrocatalysts for electrocatalytic oxidation reactions.

It has been demonstrated that controlling the shape and size of the plasmonic metallic nanocrystals precisely can regulate their properties to meet the requirements of different reactions, for which the SPR is largely dependent on the size and shape of nanocrystals [8]. For instance, the localized surface plasmon resonance (LSPR) wavelengths of Au can be efficiently tuned from the visible light to near-infrared region by controlling the size and morphology of Au nanoparticles [9-11]. The SPR of Ag can also be controlled by adjusting the shape and size of the Ag nanoparticles [12]. Accordingly, by manipulating the compositions, sizes and morphologies of the plasmonic metals, it is possible to engineer the nanocatalysts with enhanced photoelectrocatalytic activity and durability towards various chemical reactions [13-15].

The distinctive capability of plasmonic metallic nanostructures to concentrate scatter electromagnetic fields, biosensing, or convert the energy of photons into chemical energy make them suitable for various applications [16-18]. The SPR effects have been widely reported to enhance the catalytic activities of a series of reactions

such as: water splitting [10], reduction of CO_2 [13] and degradation of organic molecules [8] among others. During these processes, the SPR effect of plasmonic metallic nanostructures play a significant role in the substantial enhancement of catalytic activities [18-20]. However, the applications of the photoelectrocatalytic processes in liquid fuel oxidation reactions induced by the SPR effects have remained unexplored.

Therefore, we herein report a facile Pt-Ag hollow nanodendrites synthesis. And the as-prepared hollow Pt-Ag nanodendrites displayed a significant enhancement in the electrocatalytic performances compared with the commercial Pt/C catalyst. These outstanding properties are attributed to the unique hollow dendritic structure as well as synergistic and electronic effects between Pt and Ag. More importantly, we took advantage of the plasmonic Ag combination with the SPR to enhance the catalytic activity towards the oxidation of ethylene glycol (EG) by Pt-Ag hollow nanodendrites under visible light illumination. The resulting Pt_1Ag_1 nanocatalysts achieved 1.7-fold enhancements in mass and specific activities, showing a class of ideal photoelectrocatalysts towards liquid fuel oxidation.

2. Experimental section

2.1 Chemicals

Silver nitrate ($AgNO_3$, 99%), chloroplatinic acid (H_2PtCl_6, 99.9%), hexadecyltrimethylammonium chloride (CTAC, 99%), L-ascorbic acid (AA, $C_6H_8O_6$, 99 %), potassium hydroxide (KOH), dehydrate trisodium citrate ($Na_3C_6H_5O_7{\cdot}2\,H_2O$), acetone ($C_3H_6O$, 99 %), ethanol ($C_2H_5OH$, A.R. grade, > 99.5 %) and EG ($(CH_2OH)_2$, A.R. grade, > 99.5 %) were purchased from Sinopharm Chemicals Reagent Co., Ltd, China. Doubly distilled water was used throughout the experiments.

2.2 Preparation of Pt-Ag hollow nanodendrites

The Ag seeds were firstly prepared according to the method described by our previously reported work [21]. In the standard synthesis of Pt-Ag hollow nanodendrites, 1.4 mL H_2PtCl_6 (7.7 mM) was firstly injected into 10 mL aqueous solution in a glass vial, which contained 10 mg CTAC. After vigorous stirring for 10

min, 4 mL of AA (10 mg) was added dropwise to the above solution to serve as the reducing agent. After continuous reaction for 3 min, 5 mL of freshly-prepared Ag seeds were dropped into this aqueous solution. Then, the aqueous solution was violently shaken and capped, and then sonicated at ambient temperature for another 2 h. For comparison, the $Pt_1Ag_{0.5}$ and $Pt_1Ag_{1.5}$ hollow nanodendrites were also prepared by tuning the amounts of Ag seeds to 2.5 and 7.5 mL, respectively, while keeping the other reaction parameters unchanged.

2.3 Characterizations

In this work, we firstly used the Tecnai G220 (FEI America) to investigate the morphology and structure of the samples. After that, the FEI Tecnai F20 transmission electron microscope operated at an accelerating voltage of 200 kV was employed to record the scanning transmission electron microscopy (STEM), high-magnification transmission electron microscopy (HR-TEM) and EDX elemental mapping images. An X'Pert-Pro MPD diffractometer (Netherlands PANalytical) with a Cu Kα X-ray source (λ = 1.540598 Å) was used to obtain the powder X-ray diffraction (PXRD) patterns of the samples. The compositions and elemental valences were characterized by X-ray photoelectron spectroscopy (XPS), which was performed on a VG Scientific ESCALab 220XL electron spectrometer using 300 W Al Kα radiation.

2.4 Electrochemical measurements

Cyclic voltammetry (CV) was employed to investigate the electrocatalytic performances carried out in a standard three-electrode system, which included a Pt wire, glassy carbon electrode (GCE), a saturated calomel electrode (SCE) and as counter, working and reference electrodes, respectively. In the standard preparation of catalysts-coated electrode, the catalysts should firstly be re-dispersed in a mixture solvent containing Nafion and isopropanol and to form a homogeneous catalyst ink by sonicating for 30 min. Next, five microlitres of the dispersion was transferred onto the GC electrode and dried naturally. The CV was operated using in 1 M KOH + 1 M EG at the potential ranging from -0.9 to 0.3 V with the sweeping rate of 50 mV/s. Every time before examination, the GCE was polished with alumina powder and then rinsed with doubly deionized water and ethanol for several times. Besides, the measurements

of successive CVs of 500 cycles were also conducted for investigating their long-term durability. To achieve precise results, all the electrochemical measurements were repeated five times. The photocurrent responses of the modified electrode in 1 M EG + KOH solution were measured with a potential of −0.2 V at a scan rate of 50 mV s^{-1} under visible light illumination. The illumination was interrupted every 100 s. Electrochemical impedance spectroscopy (EIS) measurements were carried out at -0.2 V with an AC perturbation signal of 5.0 mV over the frequency range from 100 kHz to 0.1 Hz. It was worth noting that all the visible light in particular, photo-electrochemical measurements were operated by using a xenon lamp (150 W) with UV cut–off filter (>400 nm) at the distance of 28 cm to irradiate all the working electrodes.

3. Results and discussion

3.1 Materials characterizations

The unique Pt-Ag hollow nanodendrites have been prepared by employing a facile wet-chemical method, where CTAC and AA serve as the stabilizers and reducing agents, respectively (See the Experimental Section for details). The as-obtained products were firstly characterized by employing the TEM. The morphological and structural features were characterized *via* TEM and HAADF-STEM. Fig.1a and b show that the products consist of the uniform hollow nanostructure with the dendrite-like surface. In addition, the nanocrystals were highly dispersed with an average size of 53.8 nm (Supporting Information, Fig.S1). The HRTEM image of the individual nanodendrite illustrates that the lattice fringe spacing is calculated to be 0.230 nm (Fig.1c), which is associated with the (111) facet of Pt-Ag alloy [23]. The PXRD patterns of the Pt-Ag hollow nanodendrites exhibit the typical face centered cubic (*fcc*) structure with the diffraction peaks located between those of the standard Pt and Ag (Fig.1d), which are associated with the HRTEM result, further confirming the formation of Pt-Ag alloy phases in the Pt-Ag hollow nanodendrites. The atomic ratio of Pt/Ag is 52.3/47.7, as revealed by inductively coupled plasma atomic emission spectroscopy (ICP-AES), which is also consistent with the scanning electron

microscope energy dispersive X-ray spectroscopy (SEM-EDS) (51.4/48.6, Fig.1e). Besides, the composition distribution of Pt_1Ag_1 hollow nanodendrites was investigated by employing the EDX elemental mapping analysis, where both Pt and Ag were distributed uniformly over the whole Pt-Ag hollow nanodendrite (Fig.1f), as confirmed by the line-scan analysis (Fig.1g).

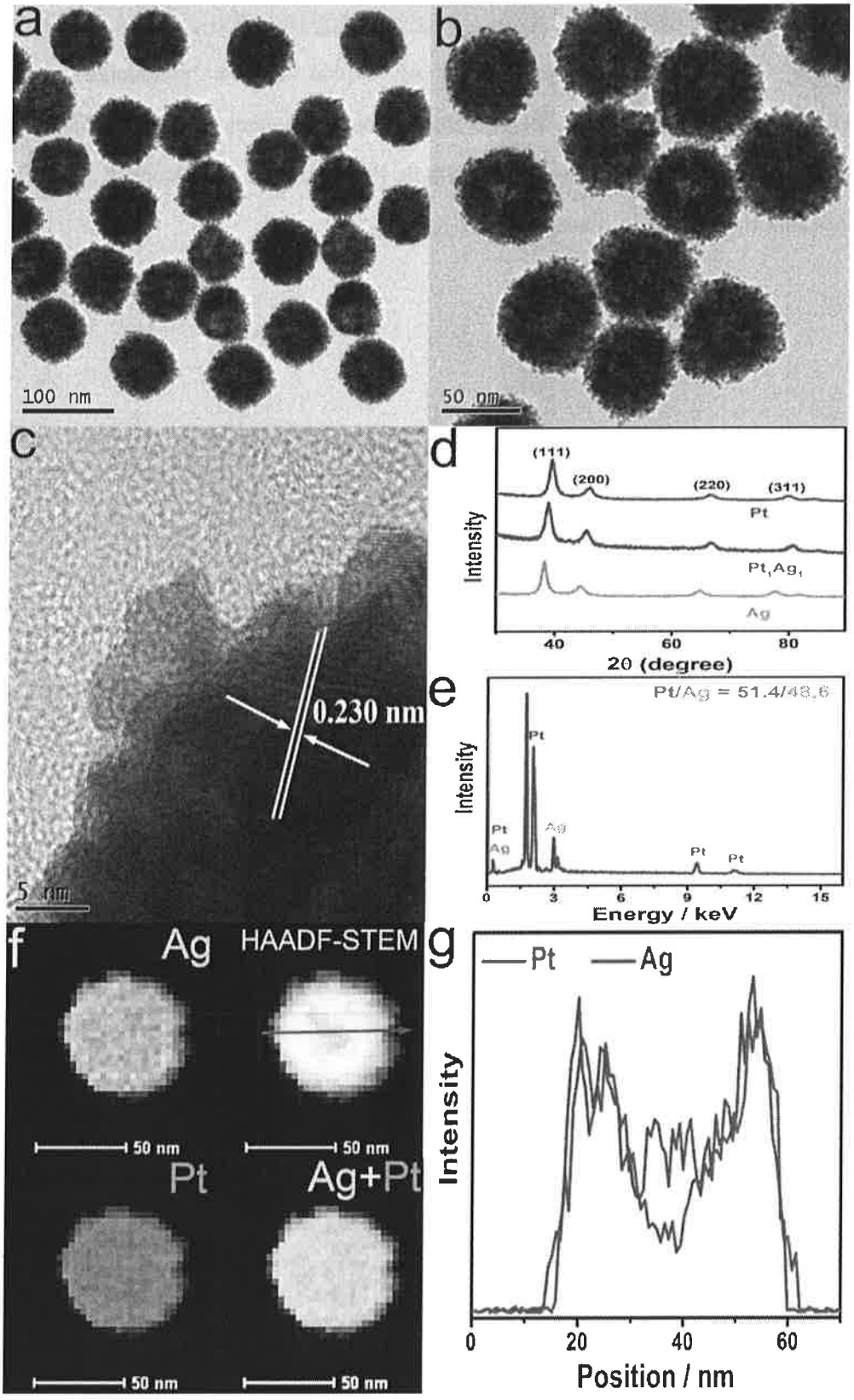

Fig.1 (a, b) Representative TEM images of Pt_1Ag_1 hollow nanodendrites with different magnifications. (c) HRTEM image of an individual Pt_1Ag_1 hollow nanodendrite. (d) XRD patterns

of Pt_1Ag_1 hollow nanodendrites, Pt and Ag. (e) The TEM-EDX elemental mapping, HAADF-STEM and corresponding (f) line-scan of individual Pt_1Ag_1 hollow nanodendrites for element distribution analyses.

Moreover, in order to understand the compositions and elemental valences of the Pt_1Ag_1 hollow nanodendrites, the XPS measurements were also employed. As displayed in Fig.2a, the typical peaks at the binding energy (B.E.) of 71.5 and 74.3 eV were assigned to the Pt $4f_{7/2}$ and Pt $4f_{5/2}$ states, respectively. The XPS of Pt $4f_{7/2}$ in the Pt_1Ag_1 hollow nanodendrites shifted positively to a higher B.E. and Ag 3d shifted to a lower B.E. compared with that of standard Pt and Ag, indicating the changes in the electronic structure, which may be attributed to the occurrence of charge transfer from Ag to Pt [24-26]. More importantly, both of the metallic states of Pt and Ag (Fig.2b) were the predominant states in Pt_1Ag_1 hollow dendrites.

Next, we analyzed the optical properties of the as-obtained Pt_1Ag_1 hollow nanodendrites, by measuring the UV–vis adsorption spectra of the samples, as is displayed in Fig.2c. The Pt_1Ag_1 hollow nanodendrites showed an absorption edge at *ca.* 420 nm, which is associated with the adsorption of Ag nanoparticles, revealing the distinct absorptions of visible light [27]. While the adsorption edge at *ca.* 650 nm may be ascribed to some unremoved residues. These results suggest that the as-prepared PtAg hollow nanodendrites catalyst possess the outstanding optical properties, which might be beneficial for photoelectrocatalytic ethylene glycol oxidation reaction (EGOR). In addition, we conducted the photocurrent response measurement to study the photoelectric properties of the resulted Pt_1Ag_1 hollow nanodendrites. Fig.2d showed the photocurrent–time (I–t) curve on the Pt_1Ag_1 hollow nanodendrites modified electrode. Remarkably, a responsive photocurrent with intensity of *ca.* 200 mA mg^{-1} was observed for the EGOR when the electrode was upon visible light illumination. Besides, the photocurrent response was also repeatable during on/off cycles upon light illumination, indicating that the SPR and electronic effects between Ag and Pt were favorable for the enhancement of current density [28].

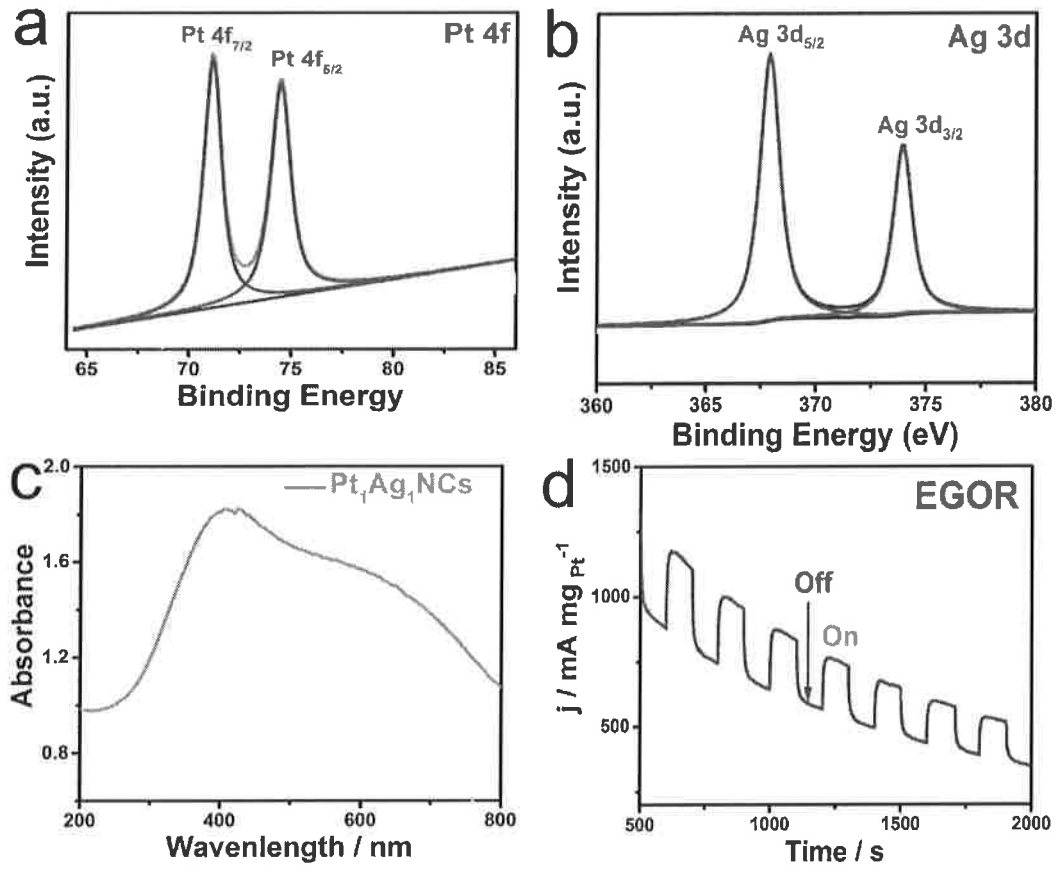

Fig. 2 The XPS spectra of (a) Pt 4f and (b) Ag 3d in Pt_1Ag_1 hollow nanodendrites. (c) UV-vis spectra of dendritic Pt_1Ag_1 hollow nanodendrites, and (d) photocurrent responses of Pt_1Ag_1 hollow nanodendrites towards EGOR in 1 M EG and 1 M KOH solution at a potential of -0.2 V under visible light illumination. The illumination from a Xe lamp was interrupted every 100 s.

To uncover the influences of composition on the final shape, we herein synthesized the other two types of $Pt_1Ag_{1.5}$ and $Pt_1Ag_{0.5}$ hollow nanodendrites by simply varying the amount of Ag seeds while keeping the concentration of H_2PtCl_6 solution the same. According to the Fig.S2 (Supporting Information), Pt_1Ag_1 hollow nanodendrites were similar to both $Pt_1Ag_{1.5}$ and $Pt_1Ag_{0.5}$, indicating the synthesis of Pt-Ag hollow nanodendrites was not dependable on the atomic ratio.

3.2 Electrochemical tests

The visible-light-enhanced electrocatalytic oxidation reaction can be applied due to the distinctive hollow dendritic nanostructure, optical properties and the strong SPR effects of the resulted Pt-Ag hollow nanodendrites. Therefore, we herein chose the electrocatalytic oxidation of EG to evaluate the photoelectrocatalytic properties of the dendritic Pt-Ag hollow nanodendrites under the visible light irradiation. The CV

operated in 1 M KOH solution (Fig.3a) was significant for evaluating the electrochemically active surface areas (ECSA) of the electrocatalysts, which can provide some crucial information regarding the number of available active sites. Therefore, a higher ECSA value means more available surface active sites [29, 30]. The ECSA value for Pt_1Ag_1 hollow nanodendrites was calculated to be 50.2 $m^2 g^{-1}$, which was much higher than those of $Pt_1Ag_{0.5}$ hollow nanodendrites (46.2 $m^2 g^{-1}$) and $Pt_1Ag_{1.5}$ hollow nanodendrites (48.3 $m^2 g^{-1}$) (Fig.3b). The higher ECSA of Pt_1Ag_1 hollow nanodendrites was attributed to the combination of the roughly dendritic surface and hollow nanostructures [31].

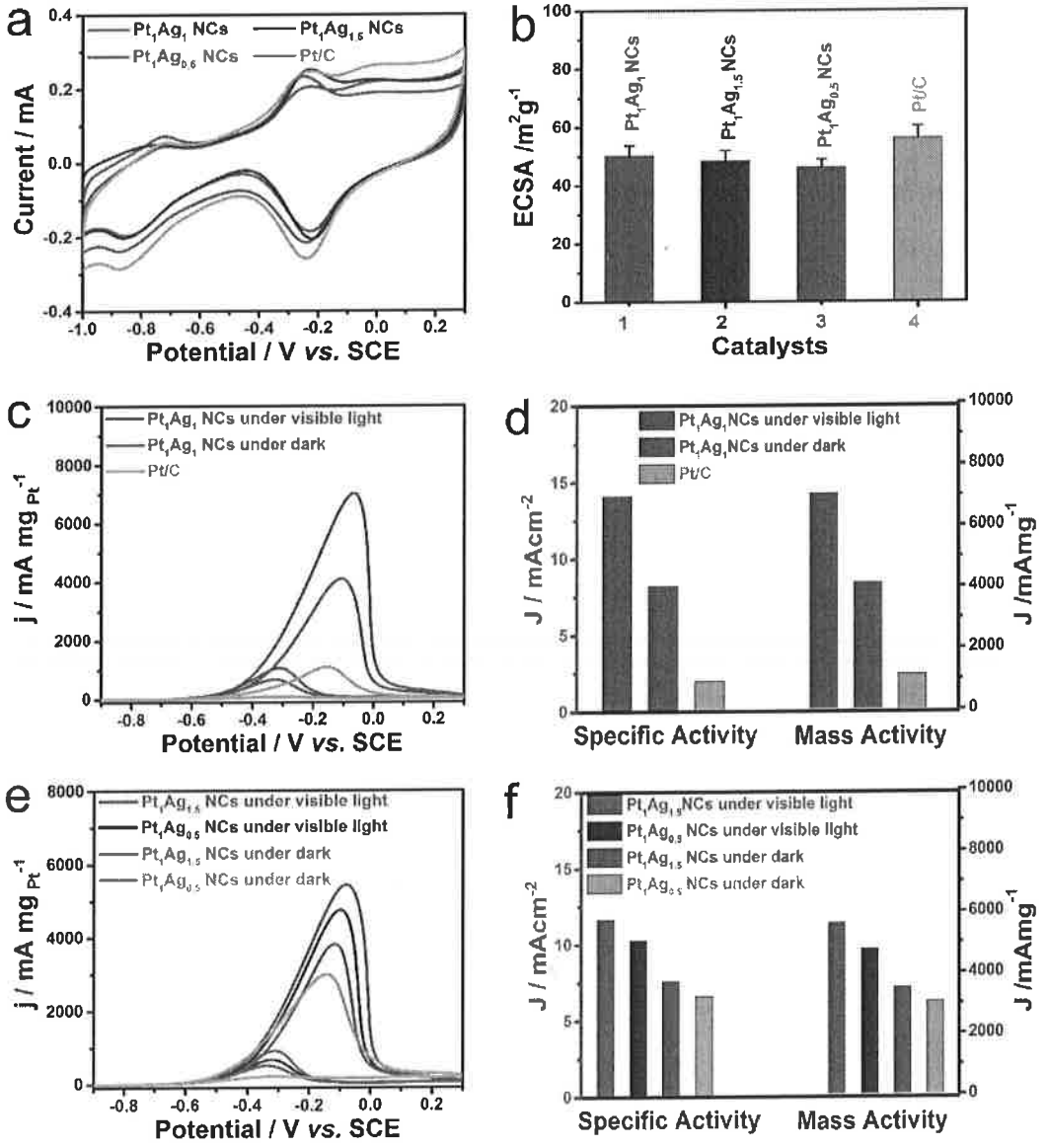

Fig. 3 (a) CV curves of Pt_1Ag_1, $Pt_1Ag_{1.5}$, $Pt_1Ag_{0.5}$ hollow nanodendrites and commercial Pt/C in 1

M KOH solution. (b) The calculated ECSA of Pt_1Ag_1, $Pt_1Ag_{1.5}$, $Pt_1Ag_{0.5}$ hollow nanodendrites and commercial Pt/C. (c) CV curves of Pt_1Ag_1 hollow nanodendrites under visible light illumination and dark, as well as commercial Pt/C. (d) The calculated specific and mass activities Pt_1Ag_1 hollow nanodendrites under visible light illumination and dark, as well as commercial Pt/C towards EGOR. (e) CV curves of $Pt_1Ag_{1.5}$, $Pt_1Ag_{0.5}$ hollow nanodendrites towards EGOR under visible light illumination and dark. (f) The calculated specific and mass activities of $Pt_1Ag_{1.5}$, $Pt_1Ag_{0.5}$ hollow nanodendrites towards EGOR under visible light illumination and dark condition were illustrated. These electrochemical measurements were repeated five times to achieve precise results.

The electrocatalytic performances of the Pt-Ag hollow nanodendrites were then carried out in 1 M KOH and 1 M EG solution at the sweeping rate of 50 mV/s. For comparison purposes, the peak current densities were normalized to both the ECSA and the mass of Pt loading on the surface of the modified electrodes. As it can be seen in Fig.3c, the Pt_1Ag_1 hollow nanodendrites displayed a remarkably superior peak current density under visible light irradiation than that under dark conditions. Fig.3d shows the histogram for the specific and mass activities of commercial Pt/C and Pt_1Ag_1 hollow nanodendrites under visible light irradiation or dark conditions. Among these, the Pt_1Ag_1 hollow nanodendrites under visible light irradiation displayed the highest mass and specific activities of 7045.2 mA mg^{-1} and 14.1 mA cm^{-2}. In addition, 6.2 and 7.0-fold enhancements were found compared to those of the commercial Pt/C (1135.2 mA mg^{-1} and 2.05 mA cm^{-2}). More interestingly, the Pt_1Ag_1 hollow nanodendrites under visible light irradiation also displayed 1.7 times higher than under dark (4129.1 mA mg^{-1} and 8.2 mA cm^{-2}).

The electrocatalytic activities of the other two types of Pt-Ag hollow nanodendrites with different compositions were also investigated. As it can be seen in Fig. 3e and f, both $Pt_1Ag_{1.5}$ and $Pt_1Ag_{0.5}$ nanocatalysts displayed excellent electrocatalytic performances towards EGOR under visible light irradiation with the specific activities found to be 11.7 and 10.3 mA cm^{-2}, which are1.54 and 1.56 times higher than those under dark conditions, respectively. Apart from the specific activity, both $Pt_1Ag_{1.5}$ and $Pt_1Ag_{0.5}$ hollow nanodendrites also displayed an enhancement in mass activity, 5628.7 mA mg^{-1} and 4756.8 mA mg^{-1} towards EGOR when the modified electrodes were upon the visible light irradiation. The electrocatalytic activities towards EGOR were enhanced greatly by the SPR effects, unique dendritic

structure and the synergistic properties between Pt and Ag [32, 33].

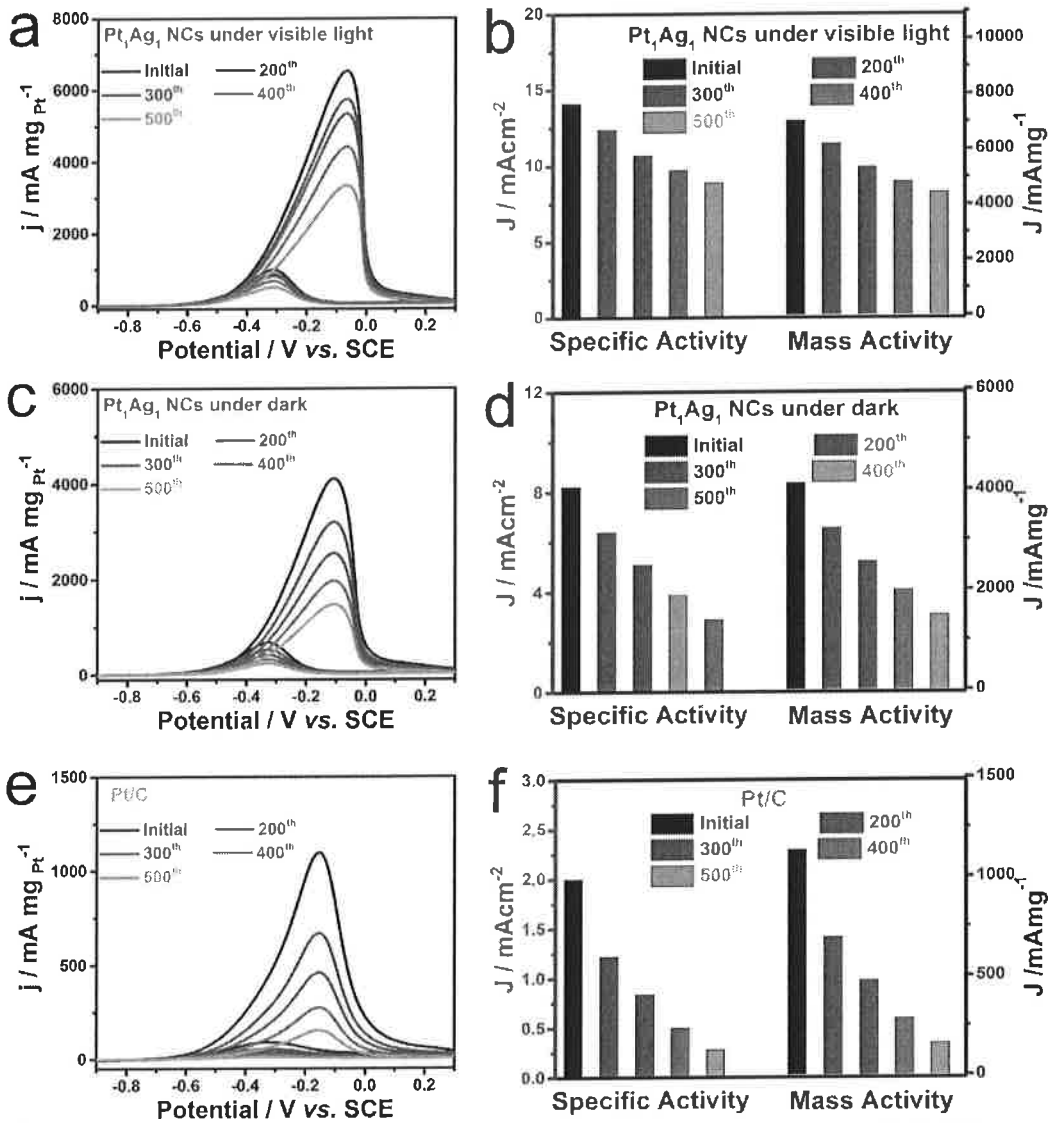

Fig.4 Durability comparison of (a and b) $Pt_1Ag_{0.5}$ hollow nanodendrites under visible light irradiation, (c and d) $Pt_1Ag_{0.5}$ hollow nanodendrites under ambient reaction and (e and f) commercial Pt/C for the successive CVs of 200th, 300th ,400th and 500th cycles together with the retained specific and mass activities. These electrochemical measurements were repeated five times to achieve precise results.

The durability of the catalyst is also another significant parameter for evaluating the properties of an electrocatalyst in fuel cells. An electrocatalyst with better durability means a much longer lifetime, which is crucial for practical applications [34]. Therefore, we conducted the continuous 500 cycles CV to investigate their electrocatalytic durability, which were carried out in the solution of 1 M KOH + 1 M EG solution. According to the Fig.4, although the peak current densities of these

catalysts decayed rapidly in the initial period, the Pt_1Ag_1 hollow nanodendrites upon the visible light irradiation displayed the slowest current decay over time and retained the highest activity among these catalysts after 500 cycles. For more detailed comparison, the normalized current densities of these electrocatalysts are also recorded. As seen, the Pt_1Ag_1 hollow nanodendrites nanocatalysts under visible light irradiation retained the catalytic activities of 63.1 % of the initial value towards EGOR, which is much higher than that of commercial Pt/C (14.3 %) and Pt_1Ag_1 hollow nanodendrites (36.2 %) under dark conditions. The retained mass and specific activities of Pt_1Ag_1 hollow nanodendrites nanocatalysts under visible light irradiation were calculated to be 4438.5 mA mg^{-1} and 8.9 mA cm^{-2}, respectively, both of which are much higher than the other electrocatalysts, indicating the superior long-term stability. The greatly enhanced durability of Pt_1Ag_1 hollow nanodendrites upon the visible light irradiation can mainly be ascribed to the highly exposed surface active sites, synergistic and electronic effects between Pt and Ag, as well as the photoelectrical synergistic effects from SPR effects.

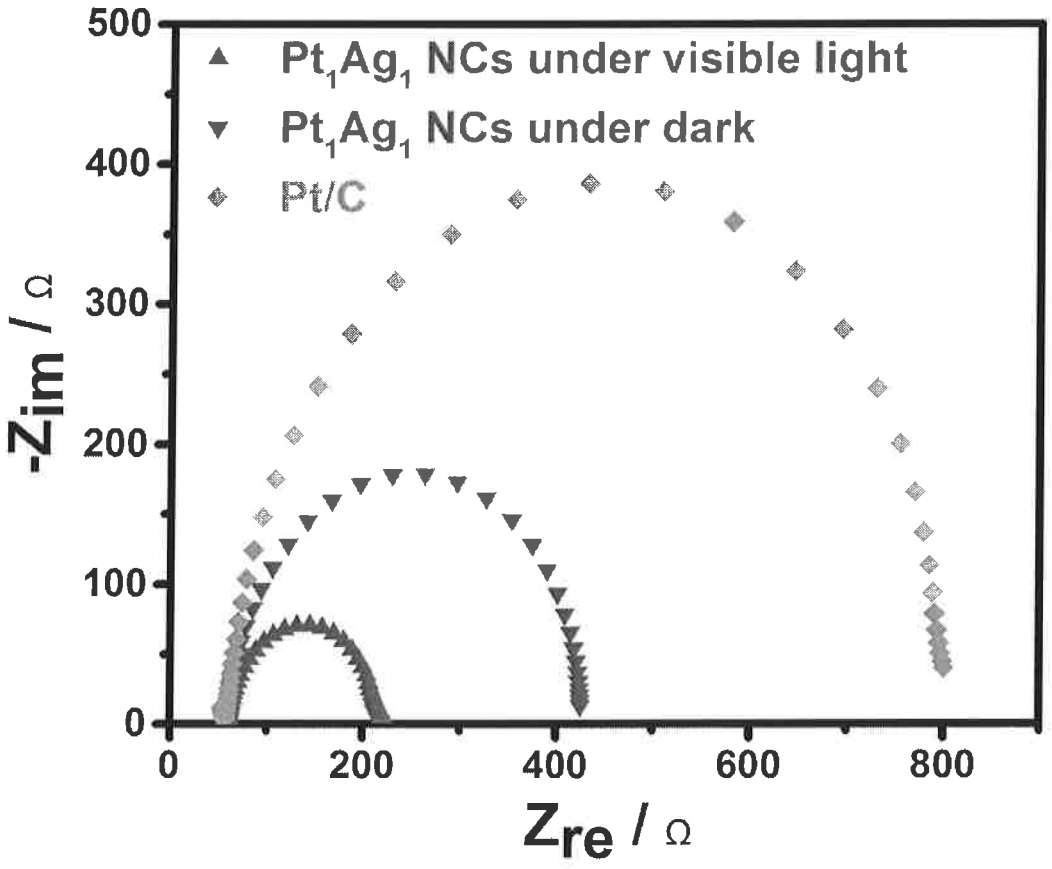

Fig.5 The Nyquist plots of commercial Pt/C, Pt_1Ag_1 hollow nanodendrites modified electrodes under visible light irradiation or dark conditions at the potential of -0.2 V.

Next, we have also conducted EIS at the potential of -0.1 V, for which the diameter is a crucial parameter, to evaluate the electrical resistance and conductivity of the as-prepared electrocatalysts. As it can be observed in Fig.5, the diameter impedance arc (DIA) of Pt_1Ag_1 hollow nanodendrites under visible light illumination is much smaller than that under dark conditions and that of the commercial Pt/C catalyst. This indicated that Pt_1Ag_1 hollow nanodendrites nanocatalysts modified electrode possessed smaller electron transfer resistance. In addition, the best electrical conductivity under visible light illumination is attributed to the SPR effect and the charge transfer between Pt and Ag [35-39].

In general, the greatly enhanced electrocatalytic performances of Pt-Ag hollow nanodendrites towards EGOR can be mainly attributed to the following combined features: (1) the unique hollow dendritic nanostructures can efficiently provide high surface active areas available for the EG molecules [40]. (2) The electronic and synergistic effects originated from the Pt and Ag are also beneficial for enhancing their electrocatalytic activity and durability [41-45]. (3) Most importantly, the photoelectrical effects induced by SPR upon the visible light irradiation are crucial for the substantial enhancements of electrocatalytic performances towards EGOR [46].

4. Conclusions

In summary, a simple method has been successfully demonstrated for the synthesis of an advanced class of Pt-Ag photoelectrocatalysts. Owing to the unique hollow nanodendrite structure, as well as the synergistic and electronic effects between Pt and Ag, the as-prepared Pt-Ag hollow nanodendrite can expose more surface active area. In addition, it can display remarkable electrocatalytic activity towards EGOR with the unprecedentedly high mass and specific activities of 7045.2 mA mg^{-1} and 14.1.1 mA cm^{-2}. Furthermore, 6.2 and 7.0-fold enhancements were obtained compared to those of the commercial Pt/C. More significantly, owing to the SPR effects based on the Ag, the Pt-Ag hollow nanodendrites under the visible light irradiation also showed an enhancement of 1.7 times in catalytic activity than that

under dark conditions. A number of excellent Pt-Ag photocatalysts have been prepared, the one we obtained is the best with both high catalytic activity and long-term stability, which can be well applied as highly efficient photoelectrocatalysts for fuel cells. This manuscript opens up a promising and novel approach for designing highly efficient photoelectrocatalysts towards liquid fuel electrooxidation and other chemical reactions, which would greatly alleviate the serious energy crisis and environment pollution.

Acknowledgements

This work was supported by the National Natural Science Foundation of China (Grant No. 51373111), the Suzhou Industry (SYG201636), the project of scientific and technologic infrastructure of Suzhou (SZS201708), the Priority Academic Program Development of Jiangsu Higher Education Institutions (PAPD).

References

[1] S. Linic, P. Christopher, D.B. Ingram, Plasmonic-metal nanostructures for efficient conversion of solar to chemical energy, Nature Mater. 10 (2011) 911-921.

[2] R. Jiang, B. Li, C. Fang, J. Wang, Metal/Semiconductor hybrid nanostructures for plasmon-enhanced applications, Adv. Mater. 26 (2014) 5274-5309.

[3] P. Christopher, H. Xin, S. Linic, Visible-light-enhanced catalytic oxidation reactions on plasmonic silver nanostructures, Nature Chem. 3 (2011) 467-472.

[4] P. Christopher, H. Xin, A. Marimuthu, S. Linic, Singular characteristics and unique chemical bond activation mechanisms of photocatalytic reactions on plasmonic nanostructures, Nature Mater. 11 (2012) 1044-1050.

[5] H. Yang, L.Q. He, Y.W. Hu, X. Lu, G.R. Li, B. Liu, B. Ren, Y. Tong, P.P. Fang, Quantitative Detection of Photothermal and Photoelectrocatalytic Effects Induced by SPR from Au@Pt Nanoparticles, Angew. Chem. 54 (2015) 11462-11466.

[6] C. Clavero, Plasmon-induced hot-electron generation at nanoparticle/metal-oxide interfaces for photovoltaic and photocatalytic devices, Nature Photo. 8 (2014) 95-103.

[7] S.K. Cushing, J. Li, F. Meng, T.R. Senty, S. Suri, M. Zhi, M. Li, A.D. Bristow, N. Wu, Photocatalytic activity enhanced by plasmonic resonant energy transfer from metal to semiconductor, J. Am. Chem. Soc. 134 (2012) 15033-15041.

[8] Z. Zheng, T. Tachikawa, T. Majima, Plasmon-enhanced formic acid dehydrogenation using anisotropic Pd-Au nanorods studied at the single-particle level, J. Am. Chem. Soc. 137 (2015) 948-957.

[9] Z. Zhang, A. Li, S.W. Cao, M. Bosman, S. Li, C. Xue, Direct evidence of plasmon enhancement on photocatalytic hydrogen generation over Au/Pt-decorated TiO_2 nanofibers, Nanoscale 6 (2014) 5217-5222.

[10] B.-H. Wu, W.-T. Liu, T.-Y. Chen, T.-P. Perng, J.-H. Huang, L.-J. Chen, Plasmon-enhanced photocatalytic hydrogen production on Au/TiO_2 hybrid

nanocrystal arrays, Nano Energy 27 (2016) 412-419.
[11] Z. Lou, M. Fujitsuka, T. Majima, Pt-Au triangular nanoprisms with strong dipole plasmon resonance for hydrogen generation studied by single-particle spectroscopy, ACS nano 10 (2016) 6299-6305.
[12] H. Zhang, X. Fan, X. Quan, S. Chen, H. Yu, Graphene sheets grafted Ag@AgCl hybrid with enhanced plasmonic photocatalytic activity under visible light, Environ. Sci. Technol. 45 (2011) 5731-5736.
[13] K.M. Choi, D. Kim, B. Rungtaweevoranit, C.A. Trickett, J.T. Barmanbek, A.S. Alshammari, P. Yang, O.M. Yaghi, Plasmon-enhanced photocatalytic $CO_{(2)}$ conversion within metal-organic frameworks under visible light, J. Am. Chem. Soc. 139 (2017) 356-362.
[14] S. Bai, X. Li, Q. Kong, R. Long, C. Wang, J. Jiang, Y. Xiong, Toward enhanced photocatalytic oxygen evolution: synergetic utilization of plasmonic effect and schottky junction via interfacing facet selection, Adv. Mater. 27 (2015) 3444-3452.
[15] F. Wang, C. Li, H. Chen, R. Jiang, L.D. Sun, Q. Li, J. Wang, J.C. Yu, C.H. Yan, Plasmonic harvesting of light energy for suzuki coupling reactions, J. Am. Chem. Soc. 135 (2013) 5588-5601.
[16] J. Xue, S. Ma, Y. Zhou, Z. Zhang, M. He, Facile Photochemical synthesis of Au/Pt/g-C_3N_4 with Plasmon-enhanced photocatalytic activity for antibiotic degradation, ACS Appl. Mater. Interfaces 7 (2015) 9630-9637.
[17] R. Shi, Y. Cao, Y. Bao, Y. Zhao, G.I.N. Waterhouse, Z. Fang, L.Z. Wu, C.H. Tung, Y. Yin, T. Zhang, Self-assembled Au/CdSe nanocrystal clusters for plasmon-mediated photocatalytic hydrogen evolution, Adv. Mater. 29 (2017) DOI: 10.1002/adma.201700803
[18] S. Liu, R. Jiang, P. You, X. Zhu, J. Wang, F. Yan, Au/Ag core–shell nanocuboids for high-efficiency organic solar cells with broadband plasmonic enhancement, Energy Environ. Sci. 9 (2016) 898-905.
[19] J. Huang, Y. Zhu, C. Liu, Y. Zhao, Z. Liu, M.N. Hedhili, A. Fratalocchi, Y. Han, Fabricating a homogeneously alloyed AuAg shell on Au nanorods to achieve strong, stable, and tunable surface plasmon resonances, Small 11 (2015) 5214-5221.
[20] A. Naldoni, F. Riboni, M. Marelli, F. Bossola, G. Ulisse, A. Di Carlo, I. Píš, S. Nappini, M. Malvestuto, M.V. Dozzi, R. Psaro, E. Selli, V. Dal Santo, Influence of TiO_2 electronic structure and strong metal–support interaction on plasmonic Au photocatalytic oxidations, Catal. Sci. Technol. 6 (2016) 3220-3229.
[21] H. Xu, J. Wang, B. Yan, K. Zhang, S. Li, C. Wang, Y. Shiraishi, Y. Du, P. Yang, Hollow Au_xAg/Au core/shell nanospheres as efficient catalysts for electrooxidation of liquid fuels, Nanoscale 9 (2017) 12996-13003.
[22] H. Xu, J. Wang, B. Yan, S. Li, C. Wang, Y. Shiraishi, P. Yang, Y. Du, Facile construction of fascinating trimetallic PdAuAg nanocages with exceptional ethylene glycol and glycerol oxidation activity, Nanoscale 9 (2017) 17004-17012.
[23] Krittayavathananon A, Sawangphruk M, et al. Electrocatalytic oxidation of ethylene glycol on palladium coated on 3D reduced graphene oxide aerogel paper in alkali media: Effects of carbon supports and hydrodynamic diffusion. Electrochim Acta 2016;212;237-246.

[24] Xu H, Yan B, Li S, Wang J, Song P, Wang C, et al. Highly open bowl-like PtAuAg nanocages as robust electrocatalysts towards ethylene glycol oxidation. J Power Sources. 2018;384:42-47.
[25] J. B. Xu, T. S. Zhao, Z. X. Liang, synthesis of active platinum-silver alloy electrocatalyst toward the formic acid oxidation reaction, J. Phys. Chem. C 112 (2008) 17362–17367
[26] Y.Y. Feng, G.R. Zhang, J.H. Ma, G. Liu, B.Q. Xu, Carbon-supported Pt^Ag nanostructures as cathode catalysts for oxygen reduction reaction, PCCP 13 (2011) 3863-3872.
[27] J. Fei, J. Li, Controlled preparation of porous TiO_2-Ag nanostructures through supramolecular assembly for plasmon-enhanced photocatalysis, Adv. Mater. 27 (2015) 314-319.
[28] M. Zhu, C. Zhai, M. Sun, Y. Hu, B. Yan, Y. Du, Ultrathin graphitic C_3N_4 nanosheet as a promising visible-light-activated support for boosting photoelectrocatalytic methanol oxidation, Appl. Catal. Environ. 203 (2017) 108-115.
[29] H. Xu, B. Yan, K. Zhang, J. Wang, S. Li, C. Wang, Y. Shiraishi, Y. Du, P. Yang, Ultrasonic-assisted synthesis of N-doped graphene-supported binary PdAu nanoflowers for enhanced electro-oxidation of ethylene glycol and glycerol, Electrochim. Acta 245 (2017) 227-236.
[30] Sawangphruk M, Krittayavathananon A, Chinwipas N. Ultraporous palladium on flexible graphene-coated carbon fiber paper as high-performance electro-catalysts for the electro-oxidation of ethanol. J Mater Chem A. 2013;1:1030-1034.
[31] H. Xu, K. Zhang, B. Yan, J. Wang, C. Wang, S. Li, Z. Gu, Y. Du, P. Yang, Ultra-uniform PdBi nanodots with high activity towards formic acid oxidation, J. Power Sources 356 (2017) 27-35.
[32] X. Weng, Q. Liu, J.J. Feng, J. Yuan, A.J. Wang, Dendrite-like PtAg alloyed nanocrystals: Highly active and durable advanced electrocatalysts for oxygen reduction and ethylene glycol oxidation reactions, J. Colloid Interface Sci. 504 (2017) 680-687.
[33] P. Song, L. Liu, J.-J. Feng, J. Yuan, A.-J. Wang, Q.-Q. Xu, Poly(ionic liquid) assisted synthesis of hierarchical gold-platinum alloy nanodendrites with high electrocatalytic properties for ethylene glycol oxidation and oxygen reduction reactions, Int. J. Hydrogen Energy 41 (2016) 14058-14067.
[34] Xu H, Song P, Fernandez C, Wang J, Zhu M, Shiraishi Y, et al. Sophisticated construction of binary PdPb alloy nanocubes as robust electrocatalysts toward ethylene glycol and glycerol oxidation. ACS Appl Mater Interfaces. 2018;10:12659-12665.
[35] G. Fu, H. Liu, N. You, J. Wu, D. Sun, L. Xu, Y. Tang, Y. Chen, Dendritic platinum–copper bimetallic nanoassemblies with tunable composition and structure: Arginine-driven self-assembly and enhanced electrocatalytic activity, Nano Res. 9 (2016) 755-765.
[36] H. Xu, B. Yan, J. Wang, K. Zhang, S. Li, Z. Xiong, C. Wang, Y. Shiraishi, Y. Du, P. Yang, Self-supported porous 2D AuCu triangular nanoprisms as model electrocatalysts for ethylene glycol and glycerol oxidation, J. Mater. Chem. A 5 (2017)

15932-15939.
[37] M.S. Hamdy, M.A. Eissa, S.M.A.S. Keshk, New catalyst with multiple active sites for selective hydrogenolysis of cellulose to ethylene glycol, Green Chem. 19 (2017) 5144-5151.
[38] H. Xu, B. Yan, K. Zhang, J. Wang, S. Li, C. Wang, Z. Xiong, Y. Shiraishi, Y. Du, P. Yang, Sophisticated construction of hollow Au–Ag–Cu nanoflowers as highly efficient electrocatalysts toward ethylene glycol oxidation, ACS Sustain. Chem. Eng. 5 (2017) 10490-10498.
[39] J. Liu, G. Xu, B. Liu, J. Zhang, A dendritic core-shell Cu@PtCu alloy electrocatalyst resulting in an enhanced electron transfer ability and boosted surface active sites for an improved methanol oxidation reaction, Chem.l Commun. 53 (2017) 7457-7460.
[40] X. Jiang, X. Yan, W. Ren, Y. Jia, J. Chen, D. Sun, L. Xu, Y. Tang, Porous AgPt@Pt nanooctahedra as an efficient catalyst toward formic acid oxidation with predominant dehydrogenation pathway, ACS Appl. Mater.Interfaces 8 (2016) 31076-31082.
[41] H. Xu, B. Yan, K. Zhang, J. Wang, S. Li, C. Wang, Y. Shiraishi, Y. Du, P. Yang, Facile fabrication of novel PdRu nanoflowers as highly active catalysts for the electrooxidation of methanol, J. Colloid Interface Sci. 505 (2017) 1-8.
[42] H. Xu, B. Yan, K. Zhang, C. Wang, J. Zhong, S. Li, P. Yang, Y. Du, Facile synthesis of Pd-Ru-P ternary nanoparticle networks with enhanced electrocatalytic performance for methanol oxidation, Int. J. Hydrogen Energy 42 (2017) 11229-11238.
[43] C. Wang, R. Yue, H. Wang, C. Zou, J. Du, F. Jiang, Y. Du, P. Yang, C. Wang, Dendritic Ag@Pt core–shell catalyst modified with reduced graphene oxide and titanium dioxide: Fabrication, characterization, and its photo-electrocatalytic performance, Int. J. Hydrogen Energy 39 (2014) 5764-5771.
[44] C.T. Lin, M.H. Shiao, M.N. Chang, N. Chu, Y.W. Chen, Y.H. Peng, B.H. Liao, H.J. Huang, C.N. Hsiao, F.G. Tseng, A facile approach to prepare silicon-based Pt-Ag tubular dendritic nano-forests (tDNFs) for solar-light-enhanced methanol oxidation reaction, Nanoscale Res. Lett. 10 (2015) 74. DOI 10.1186/s11671-015-0791-9
[45] Xu H, Yan B, Zhang K, Wang J, Li S, Wang C, et al. Sub-5nm monodispersed PdCu nanosphere with enhanced catalytic activity towards ethylene glycol electrooxidation. Electrochim Acta. 2018;261:521-9.
[46] Xu H, Yan B, Zhang K, Wang J, Li S, Wang C, et al. Self-supported worm-like PdAg nanoflowers as efficient electrocatalysts towards ethylene glycol oxidation. ChemElectroChem. 2017;4:2527-2534.

Figure

Fig.1 (a, b) Representative TEM images of Pt_1Ag_1 hollow nanodendrites with different magnifications. (c) HRTEM image of an individual Pt_1Ag_1 hollow nanodendrite. (d) XRD patterns of Pt_1Ag_1 hollow nanodendrites, Pt and Ag. (e) The TEM-EDX elemental mapping, HAADF-STEM and corresponding (f) line-scan of individual Pt_1Ag_1 hollow nanodendrites for element distribution analyses.

Fig. 2 The XPS spectra of (a) Pt 4f and (b) Ag 3d in Pt_1Ag_1 hollow nanodendrites. (c) UV-vis spectra of dendritic Pt_1Ag_1 hollow nanodendrites, and (d) photocurrent responses of Pt_1Ag_1 hollow nanodendrites towards EGOR in 1 M EG and 1 M KOH solution at a potential of -0.2 V under visible light illumination. The illumination from a Xe lamp was interrupted every 100 s.

Fig. 3 (a) CV curves of Pt_1Ag_1, $Pt_1Ag_{1.5}$, $Pt_1Ag_{0.5}$ hollow nanodendrites and commercial Pt/C in 1 M KOH solution. (b) The calculated ECSA of Pt_1Ag_1, $Pt_1Ag_{1.5}$, $Pt_1Ag_{0.5}$ hollow nanodendrites and commercial Pt/C. (c) CV curves of Pt_1Ag_1 hollow nanodendrites under visible light illumination and dark, as well as commercial Pt/C. (d) The calculated specific and mass activities Pt_1Ag_1 hollow nanodendrites under visible light illumination and dark, as well as commercial Pt/C towards EGOR. (e) CV curves of $Pt_1Ag_{1.5}$, $Pt_1Ag_{0.5}$ hollow nanodendrites towards EGOR under visible light illumination and dark. (f) The calculated specific and mass activities of $Pt_1Ag_{1.5}$, $Pt_1Ag_{0.5}$ hollow nanodendrites towards EGOR under visible light illumination and dark condition were illustrated. These electrochemical measurements were repeated five times to achieve precise results.

Fig.4 Durability comparison of (a and b) $Pt_1Ag_{0.5}$ hollow nanodendrites under visible light irradiation, (c and d) $Pt_1Ag_{0.5}$ hollow nanodendrites under ambient reaction and (e and f) commercial Pt/C for the successive CVs of 200^{th}, 300^{th} ,400^{th} and 500^{th} cycles together with the retained specific and mass activities. These electrochemical measurements were repeated five times to achieve precise results.

Fig.5 The Nyquist plots of commercial Pt/C, Pt_1Ag_1 hollow nanodendrites modified electrodes under visible light irradiation or dark conditions at the potential of -0.2 V.

Fig.1

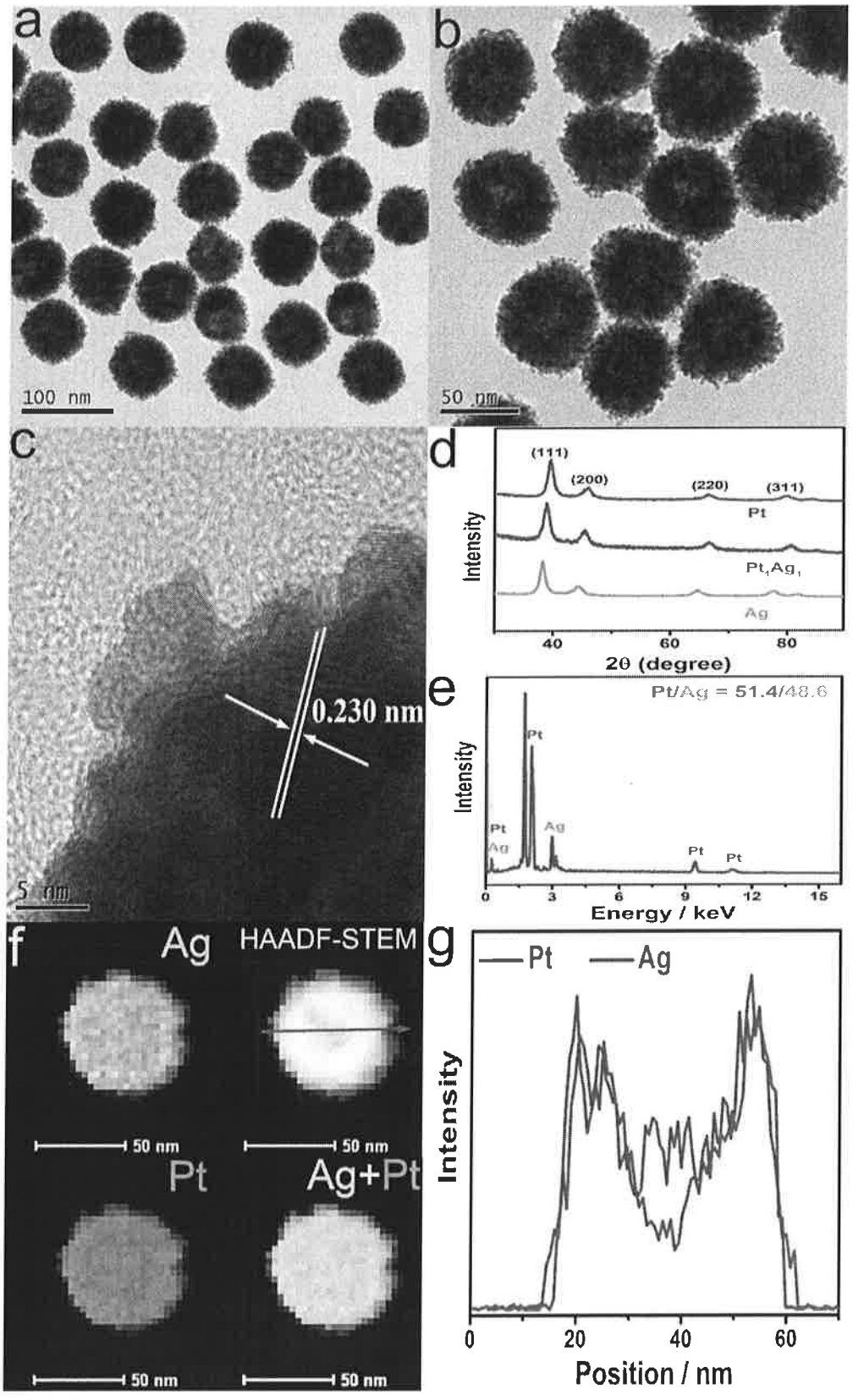
a
100 nm
b
50 nm
c
0.230 nm
5 nm
d
(111)
(200)
(220)
(311)
Pt
Pt1Ag1
Ag
Intensity
40
60
80
2θ (degree)
e
Pt/Ag = 51.4/48.6
Pt
Ag
Intensity
0
3
6
9
12
15
Energy / keV
f
Ag
HAADF-STEM
50 nm
50 nm
Pt
Ag+Pt
50 nm
50 nm
g
Pt
Ag
Intensity
0
20
40
60
Position / nm

Fig.2

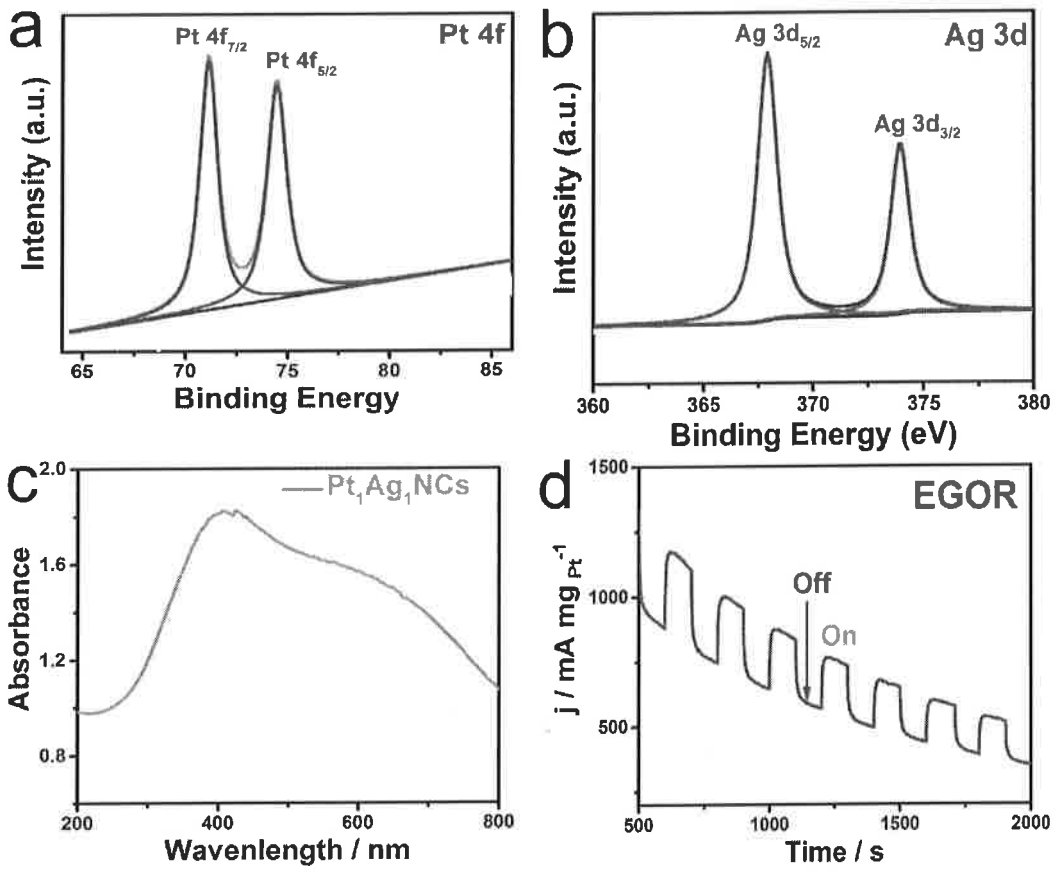
a
Pt 4f
Pt 4f7/2
Pt 4f5/2
Intensity (a.u.)
65
70
75
80
85
Binding Energy
b
Ag 3d
Ag 3d5/2
Ag 3d3/2
Intensity (a.u.)
360
365
370
375
380
Binding Energy (eV)
c
Pt1Ag1NCs
Absorbance
2.0
1.6
1.2
0.8
200
400
600
800
Wavenlength / nm
d
EGOR
Off
On
j / mA mg Pt-1
1500
1000
500
500
1000
1500
2000
Time / s

Fig.3

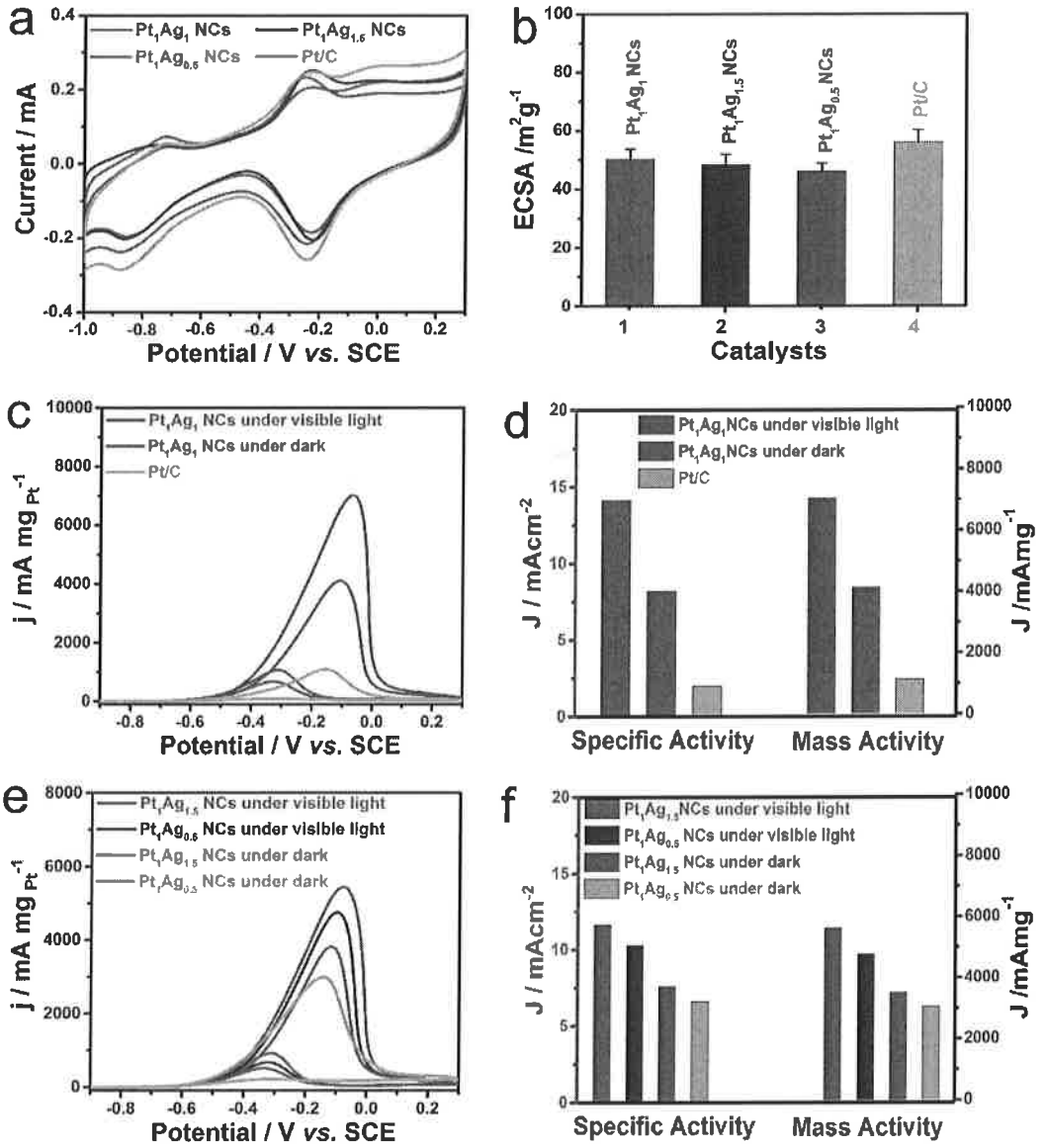
a
Pt1Ag1 NCs
Pt1Ag1.5 NCs
Pt1Ag0.5 NCs
Pt/C
Current / mA
Potential / V vs. SCE
b
ECSA /m2g-1
Pt1Ag1 NCs
Pt1Ag1.5 NCs
Pt1Ag0.5 NCs
Pt/C
Catalysts
c
Pt1Ag1 NCs under visible light
Pt1Ag1 NCs under dark
Pt/C
j / mA mgPt-1
Potential / V vs. SCE
d
Pt1Ag1NCs under visible light
Pt1Ag1NCs under dark
Pt/C
J / mAcm-2
J /mAmg-1
Specific Activity
Mass Activity
e
Pt1Ag1.5 NCs under visible light
Pt1Ag0.5 NCs under visible light
Pt1Ag1.5 NCs under dark
Pt1Ag0.5 NCs under dark
j / mA mgPt-1
Potential / V vs. SCE
f
Pt1Ag1.5NCs under visible light
Pt1Ag0.5 NCs under visible light
Pt1Ag1.5 NCs under dark
Pt1Ag0.5 NCs under dark
J / mAcm-2
J /mAmg-1
Specific Activity
Mass Activity

Fig.4

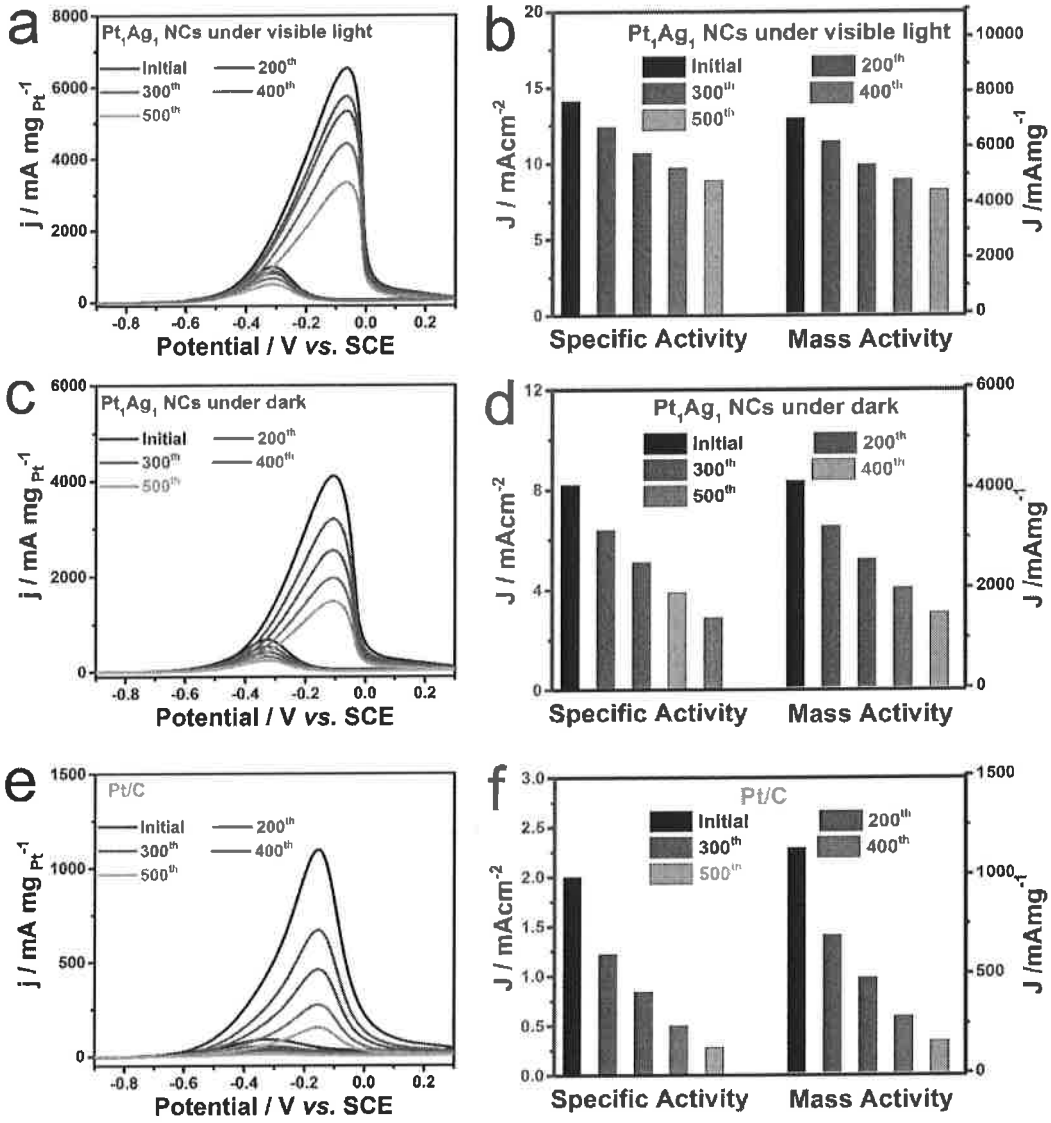
a
Pt1Ag1 NCs under visible light
Initial
200th
300th
400th
500th
j / mA mg Pt-1
Potential / V vs. SCE
b
Pt1Ag1 NCs under visible light
J / mAcm-2
J /mAmg-1
Specific Activity
Mass Activity
c
Pt1Ag1 NCs under dark
d
Pt1Ag1 NCs under dark
e
Pt/C
f
Pt/C

Fig.5

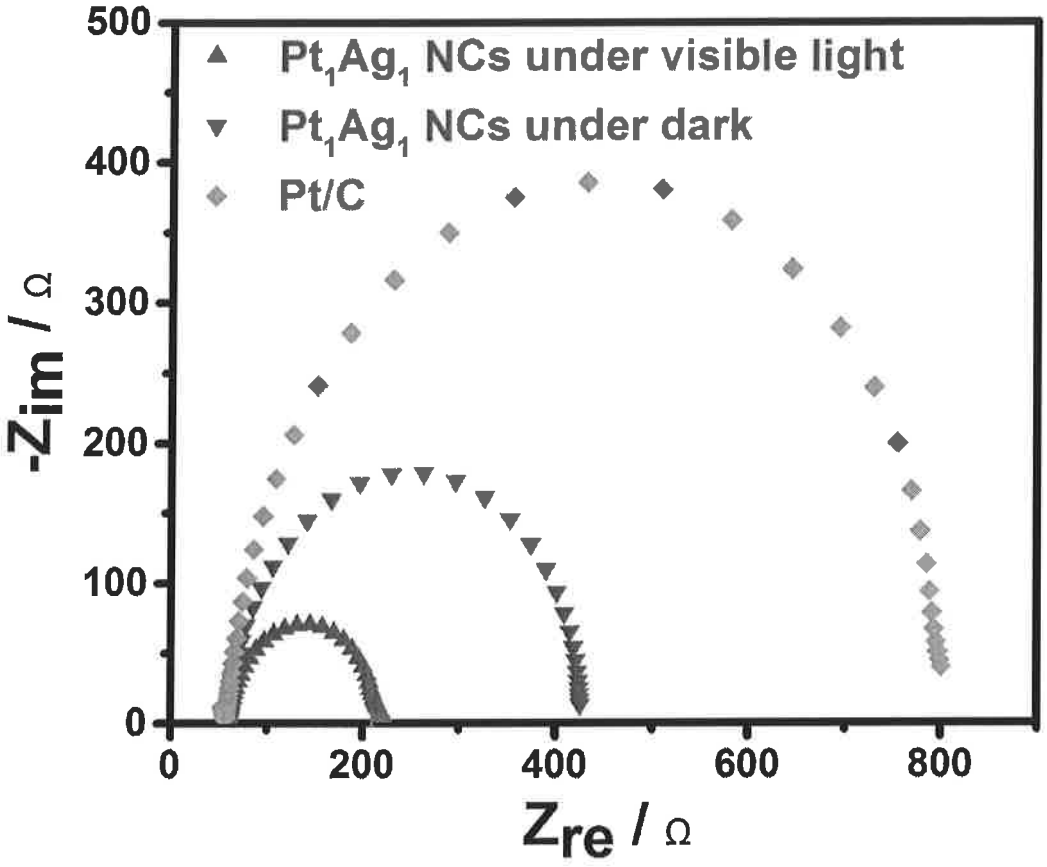
Pt1Ag1 NCs under visible light
Pt1Ag1 NCs under dark
Pt/C
-Zim / Ω
Zre / Ω
0
100
200
300
400
500
0
200
400
600
800

Supplementary Material
Click here to download Supplementary Material: Supporting Information.docx

*Graphical Abstract

Graphical Abstract